Wavelet Analysis of the Interannual Variability in Southern Québec Streamflow

FRANÇOIS ANCTIL

Département de génie civil, Pavillon Adrien-Pouliot, Université Laval, Québec, Québec, Canada

PAULIN COULIBALY

Department of Civil Engineering and School of Geography and Geology, McMaster University, Hamilton, Ontario, Canada

(Manuscript received 13 January 2003, in final form 12 May 2003)

ABSTRACT

The objectives of this study are to describe the local interannual variability in southern Québec, Canada, streamflow, based on wavelet analysis, and to identify plausible climatic teleconnections that could explain these local variations. Scale-averaged wavelet power spectra are used to simultaneously assess the interannual and spatial variability in 18 contiguous annual streamflow time series. The span of available observations, 1938–2000, allows depicting the variance for periods up to about 12 yr. The most striking feature, in the 2–3-yr band and in the 3–6-yr band—the 6–12-yr band is dominated by white noise and is not considered further—is a net distinction between the timing of the interannual variability in local western and eastern streamflows, which may be linked to the local climatology. This opens up the opportunity to construct two regional time series using principal component (PC) analysis. Then, for each band, linear relationships are sought between the regional streamflow and five selected climatic indices: the Pacific–North America (PNA), the North Atlantic Oscillation (NAO), the Northern Hemisphere annular mode (NAM), the Baffin Island–West Atlantic (BWA) and the sea surface temperature anomalies over the Niño-3 region (ENSO3). The correlation analysis revealed the presence of a change point in the streamflow time series, as reported by others, occurring around 1970. For example, the west and east 2–3-yr bands are positively correlated to PNA since 1970, which was not the case prior to that change point. The proposed regional east–west divide is particularly evident prior to 1970, with a negative NAM correlation for the west and a positive NAM (and negative ENSO3) for the east. The picture for the less energetic 3–6-yr band is mixed, with alternating dominance of teleconnection patterns, but the 1970 change point holds.

1. Introduction

Day-to-day variations of weather are to a large measure determined by the passage of atmospheric systems that vary in size, genesis, and effect depending on earth locations. Persistence of storm tracks or blockages reflects locally on the interannual variability in climatic variables, which are key elements in understanding the underlying dynamics of the hydrologic cycle. Recognition of low-frequency fluctuations leads to changes in the interpretation and utility of hydroclimatic records. The identification of coherent low-frequency patterns may also be relevant to the interpretation of long-range persistence (Rajagopalan and Lall 1998). Further, changes in the terrestrial hydrologic budget, including the amount and seasonality of precipitation, evaporation, snow water equivalent, the timing of snowmelt and runoff may influence terrestrial ecosystems (Serreze et al. 2000).

Corresponding author address: Dr. Francois Anctil, Département de génie civil, Pavillon Adrien-Pouliot, Université Laval, Québec, QC G1K 7P4, Canada.
E-mail: francois.anctil@gci.ulaval.ca

This study is concerned with southern Québec, Canada, streamflows, where the annual peak flow is usually associated with the spring snowmelt. Assessing changes in the atmospheric components of the northern midlatitude hydrologic budget is difficult, even for a standard variable such as precipitation, since the station network is fairly sparse. There are also significant problems of undercatch of solid precipitation (Woo et al. 1983). The heterogeneous nature of rainfall also asks for a large number of weather stations for an accurate characterization of rainfall patterns over large areas. Since river systems act as comprehensive integrators of precipitation over well-defined watersheds (Amarasekera et al. 1997), annual streamflow observations can serve as a pertinent index of the interannual variability in the northern midlatitude.

Fluctuations of river discharge have been associated with El Niño–Southern Oscillation events in many rivers throughout the world (e.g., Waylen and Caviedes 1990; Redmond and Koch 1991; Kahya and Dracup 1993, Dracup and Kahya 1994; Eltahir 1996; Kiem and Franks 2001). The picture for southern Québec rivers, as for many mid- and high-latitude rivers, is not as clear, and

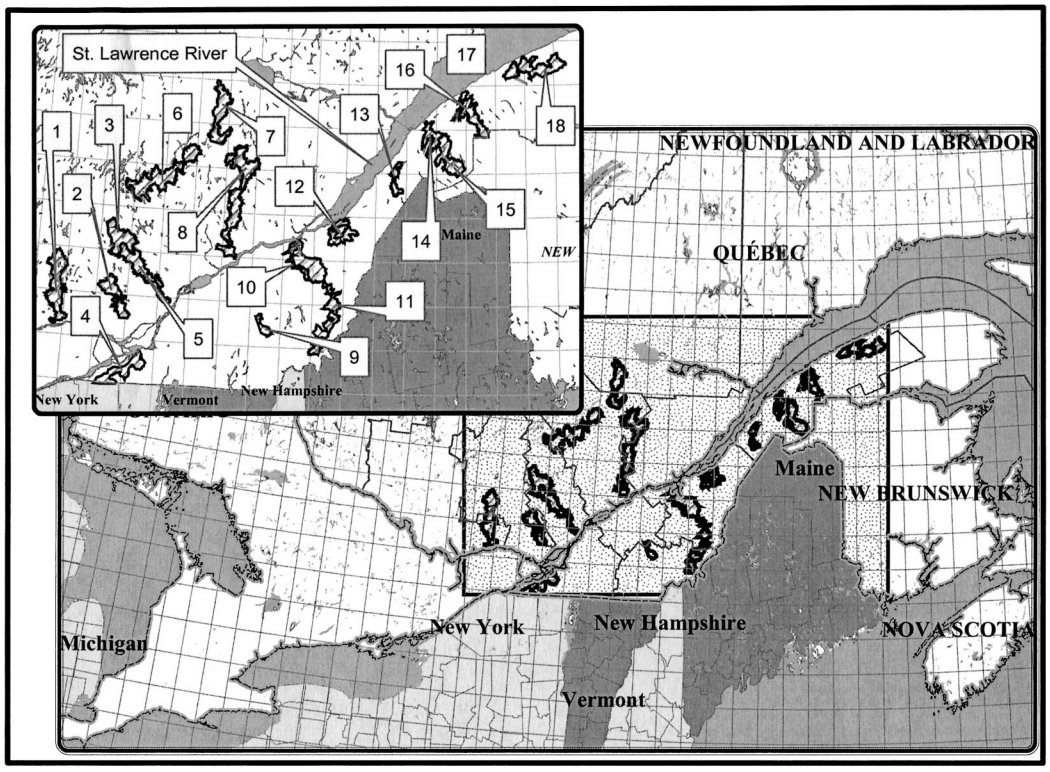

FIG. 1. Localization of the 18 selected southern Québec watersheds (Canada).

other teleconnection patterns must be sought to understand the observed interannual variability (e.g., Coulibaly et al. 2000). At the end, identification of such teleconnections could help improve long-range forecasts, which is a critical part of the development of optimal reservoir operation policies for flood control, power generation, and water supply.

Most previous interannual variability assessment studies are either based on direct correlation to identify strong statistical relationship between the climatic variable and the teleconnection pattern indices (e.g., Yarnal and Diaz 1986; Redmond and Koch 1991) or more recently on a nonparametric multitaper method of spectral analysis (Rajagopalan and Lall 1998)—a more direct measure of the occurrence process. All these approaches assume stationary time series, but continuous wavelet analysis have revealed that the interannual variability of phenomena such as El Niño–Southern Oscillation and the North Atlantic Oscillation are nonstationary, since their variance changes in frequency and intensity through time (e.g., Torrence and Compo 1998; Higuchi et al. 1999; Coulibaly et al. 2000).

The objectives of this study are to describe the local interannual variability in Southern Québec streamflow, based on wavelet analysis, and then to identify plausible teleconnections that could explain these local variations. A description of the datasets is first provided. The continuous wavelet analysis is next outlined. Results from the analysis are then reported, and finally some conclusions are drawn.

2. Datasets

The analysis is based on two types of data: streamflows and teleconnection pattern indices. Both types consist of annual means, in order to eliminate the strong seasonal variability inherent to Nordic rivers, where spring flooding lags most solid precipitation by many months.

Daily streamflow observations gathered from 18 contiguous southern Québec gauging stations are available for the proposed analysis. Figure 1 illustrates the location of the gauging stations spread along the lower St. Lawrence River and estuary, which are identified in Table 1. Continuous observations span from 1938 to 2000 (hydrological years from December to November). Watershed areas vary from 208 to 5820 km^2, while the coefficient of variation (CV) of the annual streamflows oscillates between 0.16 and 0.27. Some series are partly reconstructed, when gauging stations has been moved to a new, but near, location. There are six natural rivers in the dataset. Regulating constructions modify daily flows of the other 12 rivers, but it is believed that their annual means are unaffected since all the water stocked inside reservoirs is evacuated within the same hydrological year. The regional homogeneity of the dataset is

TABLE 1. Streamflow data analyzed.

River basin	Latitude	Longitude	Watershed area (km^2)	Flow mean ($m^3\ s^{-1}$)	Flow std div ($m^3\ s^{-1}$)	Flow CV
1 De la Petite Nation	45°47′30″N	75°05′29″W	1330	19.7	4.4	0.22
2 Du Nord	45°47′35″N	74°00′46″W	1170	23.5	4.3	0.18
3 Matawin	46°41′09″N	73°54′51″W	1390	24.2	4.3	0.18
4 Châteauguay	45°17′10″N	73°48′10″W	2460	34.3	9.2	0.27
5 L'Assomption	46°00′37″N	73°25′39″W	1340	22.9	4.4	0.19
6 Vermillon	47°39′20″N	72°57′46″W	2670	40.4	8.1	0.20
7 Croche	47°46′02″N	72°44′12″W	1570	30.6	5.4	0.18
8 Batiscan	46°32′55″N	72°24′37″W	4580	94.9	16.5	0.17
9 Nicolet Sud-Ouest	45°47′30″N	71°58′09″W	549	11.8	2.3	0.19
10 Beaurivage	46°39′33″N	71°17′19″W	709	13.8	3.1	0.22
11 Chaudière	46°35′16″N	71°12′59″W	5820	115.0	23.0	0.20
12 Du Sud	46°49′14″N	70°45′25″W	821	19.5	4.2	0.22
13 Du Loup	47°36′45″N	69°38′45″W	525	10.6	2.4	0.23
14 Des Trois-Pistoles	48°05′21″N	69°11′47″W	932	17.7	3.8	0.21
15 Madawaska	47°32′54″N	68°38′11″W	2690	49.4	9.3	0.19
16 Rimouski	48°24′48″N	68°33′22″W	1610	30.4	5.4	0.18
17 Blanche	48°46′00″N	67°39′58″W	208	4.7	1.2	0.26
18 Matane	48°46′29″N	67°32′31″W	1650	39.7	6.2	0.16

illustrated by Fig. 2, where natural rivers are described by squares and regulated ones by circles, since the coefficient of variation does not vary as a function of basin area (e.g., Smith 1992). Moreover, no systematic differences are depicted between regulated and natural river time series. The other few available time series are found strongly influenced by regulating constructions and are not included in the analysis.

Previous studies have identified several climatic patterns that appear and persist in the Northern Hemisphere. Two of these are the Pacific–North American and the North Atlantic Oscillation (NAO) that are found to be the predominant patterns for displaying low-frequency variability (interannual to decadal timescales) in the Northern Hemisphere (e.g., storm track and temperature changes; Barnston and Livezey 1987; Lamb and Peppler 1987; National Research Council 1998). The NAO is a large-scale alternation of atmospheric mass with centers of action near the Icelandic low and the Azores high. It is the dominant and persistent mode of atmospheric behavior in the North Atlantic throughout the year—explaining on average 32% of the variance in monthly sea level pressures (SLP) (Cayan 1992) but with even greater dominance during the winter. The NAO index used in this study originates from Hurrell

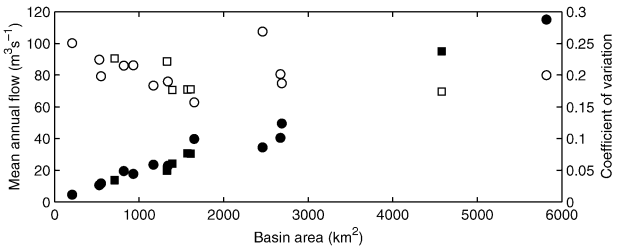

FIG. 2. Streamflow mean (black) and coef of variation (white) as a function of basin area. Natural rivers: (squares); regulated ones: (circles).

(1995) who exploited SLP anomalies from Lisbon, Portugal, and Stykkisholmur, Iceland. While exhibiting considerable interannual variability with concentrations of spectral power around periods of 2.1, 8, and 24 yr (Cook et al. 1998), the NAO has been in a generally positive phase since about 1970. A significant coherent relationship between the NAO and the North Atlantic sea surface temperature has been recently found at interannual and interdecadal timescales (Higuchi et al. 1999). The signature of the NAO is strongly regional and can be directly tied to variations in regional precipitation. Therefore the NAO index may be a relevant variable to the regional hydrology. For example, in a study on interannual variability of Canadian snow cover from 1915 to 1992 (Brown and Goodison 1996), significant winter NAO–snow-cover correlations were observed in Ontario and southern Québec, specifically in December. Another study (Brown 1995) has shown that the influence of the NAO circulation pattern on winter snow cover was mainly confined to southern Canada. Conversely, northeastern Canada seems to be dominated by the Canadian Polar trough, which is dynamically reflected by the Baffin Island–West Atlantic (BWA) pattern, as defined by Shabbar et al. (1997a) to establish more clearly the connectivity between the intensity of the western structure of the NAO at the 50-kPa-height level and the surface temperature in a region extending from 45° to 70°N. This clearly includes the present study area (Fig. 1). Coulibaly et al. (2000) have found that the BWA provides better forecast improvement for annual runoff in the northern Québec and Labrador region (a region located immediately to the north of the present study area) than the NAO. The BWA index has also been found more pertinent to explain the temperature variability in northeastern Canada than the NAO index (Shabbar et al. 1997a). Therefore, the BWA index may be an important climatic pattern to be considered in this study.

Prescribed station-based indices are now criticized, as nonoptimal representations of their time-dependent behavior of their own associated spatial patterns (Wallace 2000). For example, rather than using a prescribed station-based NAO index, one may use the leading natural mode of variability as determined from principal component analysis of the hemispheric or global SLP field, based on observations or model control runs. Thompson and Wallace (1998, 2000) worked along that path when they estimated the monthly time series of the Northern Hemisphere annular mode (NAM), originally called the Arctic Oscillation. The NAM is shown to exert a strong influence on wintertime climate throughout mid- and high-latitude continental regions, affecting not only the mean conditions, but also the day-to-day variability associated with storm intensity and the occurrence of high-latitude blocking (Thomson and Wallace 2001). The NAM is considered as a physical mode of variability of the hemispheric circulation and not an ''artifact'' of using prescribed observation stations. Wallace (2000) has shown that winter NAO can be regarded as distinct from the annular mode only if one insists upon defining it in terms of a particular station-based index. Serreze et al. (2000) consider the NAO as a major component of the NAM, with cold-season correlation of about 0.8. The NAM pattern, like the NAO, has been generally positive since the early 1970s.

Another persistent pattern that has to be considered in the Northern Hemisphere is the Pacific–North America (PNA), defined as a measure of atmospheric response to a warm sea surface temperature anomaly in the central equatorial Pacific (Wallace and Gutzler 1981). The PNA has been found to be a dominant mode of variation in the midlatitude during the winter months. It has been shown strongly related to precipitation and temperature within the same season in the western United States (Redmond and Koch 1991). Strongly positive and negative PNA indices are associated with warm events (El Niño) and cold events (La Niña), respectively, and with North American precipitation and temperature anomalies (Yarnal and Diaz 1986). It has been found that the pressure anomalies associated with the different phases of the PNA alter the normal upper-atmospheric patterns, thus affecting temperature and precipitation patterns over various regions of North America (Shabbar et al. 1997a).

In addition to the NAO, BWA, NAM, and PNA indices, indicators of the El Niño–Southern Oscillation (ENSO) are also selected for this study. The ENSO phenomenon is characterized as a spreading of warm water off the coast of South America from the equatorial central Pacific to the eastern Pacific, and is associated with climatic anomalies throughout the world. The ENSO index used in this study is the monthly mean equatorial Pacific sea surface temperatures (SST) anomalies over the Niño-3 region (5°N–5°S; 90°–150°W; Rasmusson and Carpenter 1982). For notational simplicity, ENSO3 will be used herein to denote the SST anomalies over that region. The influence of ENSO on streamflow is well documented (Waylen and Caviedes 1990; Redmond and Koch 1991; Kahya and Dracup 1993; Dracup and Kahya 1994; Eltahir 1996; Kiem and Franks 2001) and subsequently the use of the ENSO–streamflow relationship for predictive purposes has been studied extensively in recent years (Moss et al. 1994; McKerchar et al. 1996; Piechota et al. 1997, 1998; Piechota and Dracup 1999; Coulibaly et al. 2000; Gutiérrez and Dracup 2001).

It is noteworthy that some climatic indices are relatively interlinked over some time periods. As indicated previously, the BWA index is considered as a ''sister of the NAO'' (Higuchi et al. 1999); PNA and ENSO3 are connected as documented previously; and a complex relationship has been recently shown between the NAO, ENSO, and PNA patterns (Huang et al. 1998). However, a dynamical relationship between climatic patterns remains controversial and warrants further research (Shabbar et al. 1997a; Diaz et al. 2001). Therefore, the selected climatic patterns are used here as independent variables in order to find whether the proposed method can extract relevant information from a typical climatic pattern.

3. Methods

Wavelet analysis is becoming a common tool for analyzing nonstationary variance at many different frequencies within a geophysical time series (e.g., Torrence and Compo 1998; Smith et al. 1998; Labat et al. 2000), and its use is spreading to studies of the interannual variability in climate series (Shabbar et al. 1997b; Hu et al. 1998; Higuchi et al. 1999; Lucero and Rodriguez 1999; Coulibaly et al. 2000)—the following description is limited to the needs of the present study, the readers are referred to other sources, such as Labat et al. (2000), for a more thorough description of wavelet analysis capabilities in hydrology. The continuous wavelet transform W_n of a discrete sequence of observations x_n is defined as the convolution of x_n with a scaled and translated wavelet $\psi(\eta)$ that depends on a nondimensional time parameter η,

$$W_n^X(s) = \sum_{n'=0}^{N-1} x_{n'} \psi^* \left[\frac{(n' - n)\delta t}{s} \right], \qquad (1)$$

where n is the localized time index, s is the wavelet scale, δt is the sampling period, N is the number of points in the time series, and the asterik indicates the complex conjugate. Since complex wavelets lead to complex continuous wavelet transform, the wavelet power spectrum, defined as $|W_n(s)|^2$, is a convenient description of the fluctuation of the variance at different frequencies. Further, when normalized by σ^{-2} (where σ^2 is the variance), it gives a measure of the power relative to white noise, since the expectation value for a white-noise process is σ^2 at all n and s.

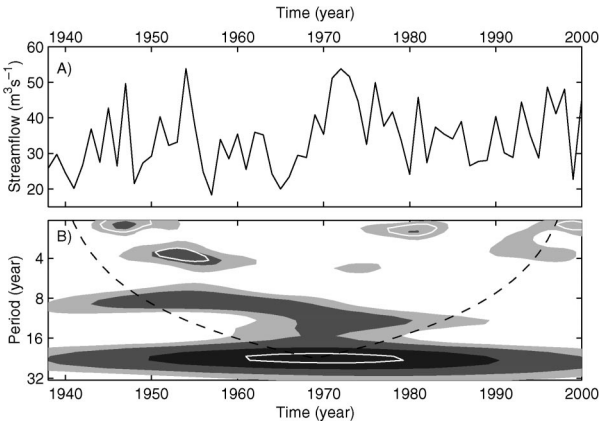

FIG. 3. Châteauguay River (No. 4 in Table 1). Time series of mean annual streamflows. (b) Normalized local wavelet power spectrum of the streamflows using the Morlet wavelet. The shaded contours are at normalized variance of 1, 2, and 4. The dashed curve depicts the cone of influence beyond which the edge effects become important. The white contour lines enclose peaks of greater than 95% confidence for a red noise with a lag-1 coef α of 0.35.

Figure 3b illustrates the normalized local wavelet power spectrum of a typical streamflow time series (Fig. 3a) using the Morlet wavelet—a complex nonorthogonal wavelet consisting of a plane wave modulated by a Gaussian:

$$\psi_0(\eta) = \pi^{-0.25} e^{i\omega_0\eta} e^{-0.5\eta^2}, \tag{2}$$

where ω_0 is the nondimensional frequency. The advantage of the Morlet wavelet over other candidates such as the Mexican hat wavelet resides in its good definition in the spectral space. For $\omega_0 = 6$ (used here), the Morlet wavelet scale is almost identical to the corresponding Fourier period of the complex exponential, and the terms scale and period may conveniently be used synonymously (Torrence and Campo 1998; Torrence and Webster 1999). The left axis in Fig. 3b is the equivalent Fourier period corresponding to the wavelet scale (hence-forth called wavelet period), and the bottom axis is time. The shaded contours are the normalized variance in excess of 1, 2, and 4. Features with variance larger than expected for a white-noise process reveal that the interannual activity is organized in preferential bands of wavelet periods. These bands, 2–3, 3–6, 6–16, and beyond 16 yr, have been reported by other investigators in precipitation and streamflow time series (Rajagopalan and Lall 1998; Coulibaly et al. 2000). This suggests the choice of the scale-averaged wavelet power to further examine fluctuations in power over specific ranges of wavelet periods (bands). Scale-averaged wavelet power is defined as the weighted sum of the wavelet power spectrum over scales s_1 to s_2:

$$\overline{W}_n^2 = \frac{\delta j \delta t}{C_\delta} \sum_{j=j_1}^{j_2} \frac{|W_n(s_j)|^2}{s_j}, \tag{3}$$

where δj is a factor that dictates the scale resolution (chosen as 0.1), and C_δ is a reconstruction factor specific to each wavelet form; $C_\delta = 0.776$ for the Morlet. This approach also allows increasing the degree of freedom of the power estimators.

In Fig. 3, the dashed curve depicts the cone of influence of the wavelet analysis (Torrence and Compo 1998). Any peaks outside the cone of influence have presumably been reduced in magnitude due to the zero padding necessary to deal with finite-length observations. For example, it is possible that activity around a period of 20 yr in Fig. 3—see, for example Hu et al. (1998) for an exploration of such period—carries on at both ends of the time series instead of diminishing as illustrated. For the span of available streamflow data, it is thus not reasonable to consider wavelet periods much beyond 12 yr. Three bands of wavelet periods are henceforth examined in greater detail: 2–3, 3–6, and 6–12.

Finally, the power spectrum produced for a given time series is the product of the natural process involved and noise. The contour lines in Fig. 3 identify peaks of greater than 95% confidence for a red-noise process with a lag-1 coefficient α of 0.35, following the Monte Carlo analysis of Torrence and Compo (1998) based on the univariate lag-1 autoregressive process. It must not be presumed that regions of the power spectrum out of these 95% confidence level areas are the product of noise only. The natural process is also present in these regions, but influences the power spectrum to a lesser extent. The coefficient α is series specific and is estimated for each series.

4. Wavelet analysis results

Scale-averaged wavelet power spectra at multiple locations allow simultaneous assessing of the spatial and temporal variability of streamflow data. Figure 4a shows a power Hovmöller (Torrence and Compo 1998), a time–longitude diagram of the normalized scale-averaged wavelet power for the streamflow observations in the 2–3-yr band (actually 2.0–3.03) at the longitude location of each gauging stations. All scale-averaged wavelet power time series [Eq. (3)] are combined in a two-dimensional contour plot, with 95% confidence level computed using the lag-1 autocorrelation at each site. To allow the juxtaposition of streamflow from watersheds of different sizes, each scale-averaged series are normalized by σ^{-2} of the original series. The zonal average of the power Hovmöller (Fig. 4b) gives a measure of the temporal fluctuation of the streamflow over the entire area. For instance, activities in the 2–3-yr band account for up to $0.7\overline{\sigma}^2$ from about 1975 to 1985, with a second but less important peak, $0.5\overline{\sigma}^2$, between 1945 and 1950. In fact, the longitudinal distribution of the power spectra of Fig. 4a reveals lots of similarities between neighboring series, but different timing between the western and eastern streamflows. A potential suspect for explaining this discrepancy is the strong oceanic influences that prevail over the eastern part of southern Québec.

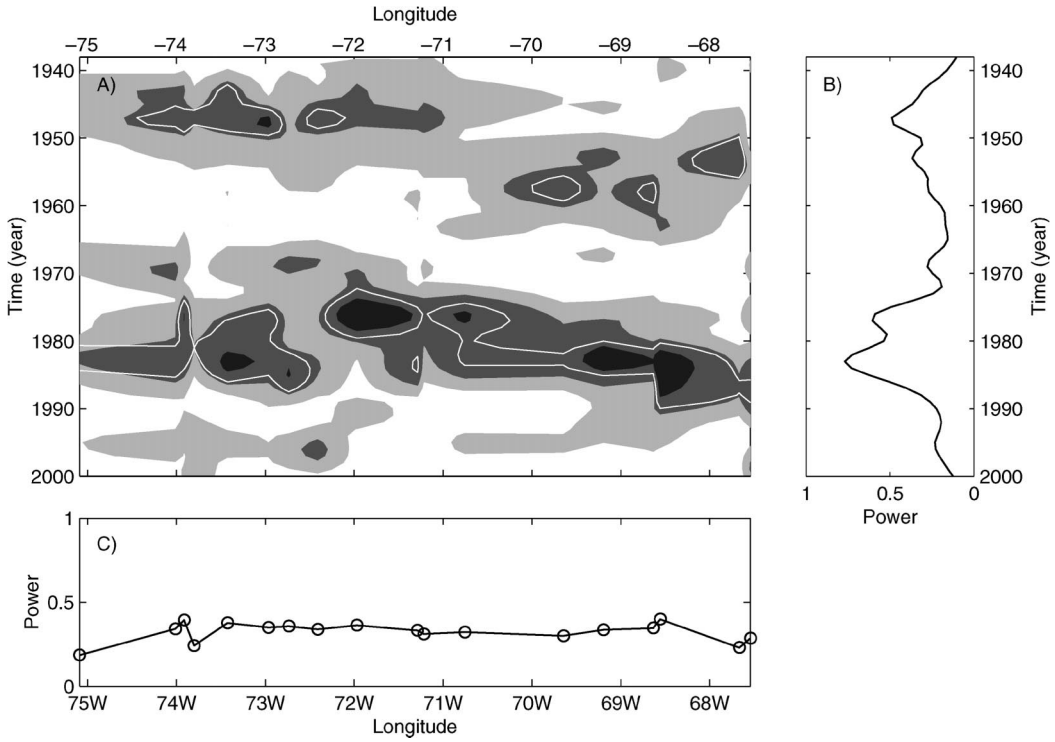

FIG. 4. Time–longitude diagrams of the streamflow observations in the 2–3-yr band. (a) Hovmöller plot of the normalized scale-averaged wavelet power. The shaded contour are at normalized power of 0.2, 0.5, and 1. The white contour lines enclose peaks of greater than 95% confidence computed using the lag-1 autocorrelation at each site. (b) Zonal avg of the power Hovmöller. (c) Temporal avg of the power Hovmöller. Circles correspond to gauging station localization.

Figure 4c illustrates the time-averaged 2–3-yr power as a function of longitude. Since all scale-averaged wavelet power series are normalized by their individual σ^{-2}, that figure does not show any striking feature except that the 2–3-yr band accounts for about $0.4\sigma^2$ at each site. Southern Québec streamflows are thus characterized by intense activity in the 2–3-yr band with peaks in the 1940s or 1950s and stronger peaks in the 1970s or 1980s, fluctuations differing as a function of longitude. Representation of time–longitude diagrams is selected for its simplicity over diagrams organized along the St. Lawrence SW–NE axis (not shown).

Figure 5 presents the power Hovmöller for the 3–6-yr band (actually 3.03–6.06). In this case, the general level of activity is less than for the precedent band (2–3-yr), since it accounts for about $0.25\sigma^2$ for western sites and $0.3\sigma^2$ for eastern sites (Fig. 5c). The 3–6-yr band shows only one peak of activity, ranging from 1940 to 1960 and attaining about $0.6\overline{\sigma}^2$ (Fig. 5b), but here again, there is a striking difference in the timing of that peak when comparing western and eastern streamflows (Fig. 5a). There has been no organized activity in that band for the last 40 yr.

The 6–12-yr band (actually 6.06–12.13) is deprived of any organized activity, as revealed by its power Hovmöller (Fig. 6). Further, its overall level of activity accounts for only about $0.1\sigma^2$. This band will not be considered further in this study since it essentially consists of white noise.

To simplify the correlation analysis between streamflows and teleconnection patterns, the longitudinal structure of the interannual variability in streamflow revealed by the power Hovmöller plots is exploited. Principal component (PC) analysis is used to construct two regional streamflow time series, one for the west and one for the east. This division roughly reflects the local climatology, which is continental in the west, and coastal in the east. In both cases, the leading PC is retained, explaining about 70% of the total variance. The PC western series (Fig. 7a) is constructed from the 10 most western ones (i.e., stations between 75.1°–71.25°W; Fig. 1), while the PC eastern series (Fig. 7b) is constructed from the 8 most eastern ones (i.e., stations between 71.25°–67.5°W; Fig. 1). The actual boundary between coastal and continental climates along the St. Lawrence River does not lie on a fixed line in space. Indeed, some of the central watersheds could have been allocated to either side without changing much the resulting PC series. The proposed organization is put forward for its simplicity and, as shown in Figs. 8 and 9, since the two PC series do preserve the main interannual features illustrated in the power Hovmöller plots for the 2–3-yr and 3–6-yr wavelet bands.

Figure 8 shows the 2–3-yr scale-averaged wavelet

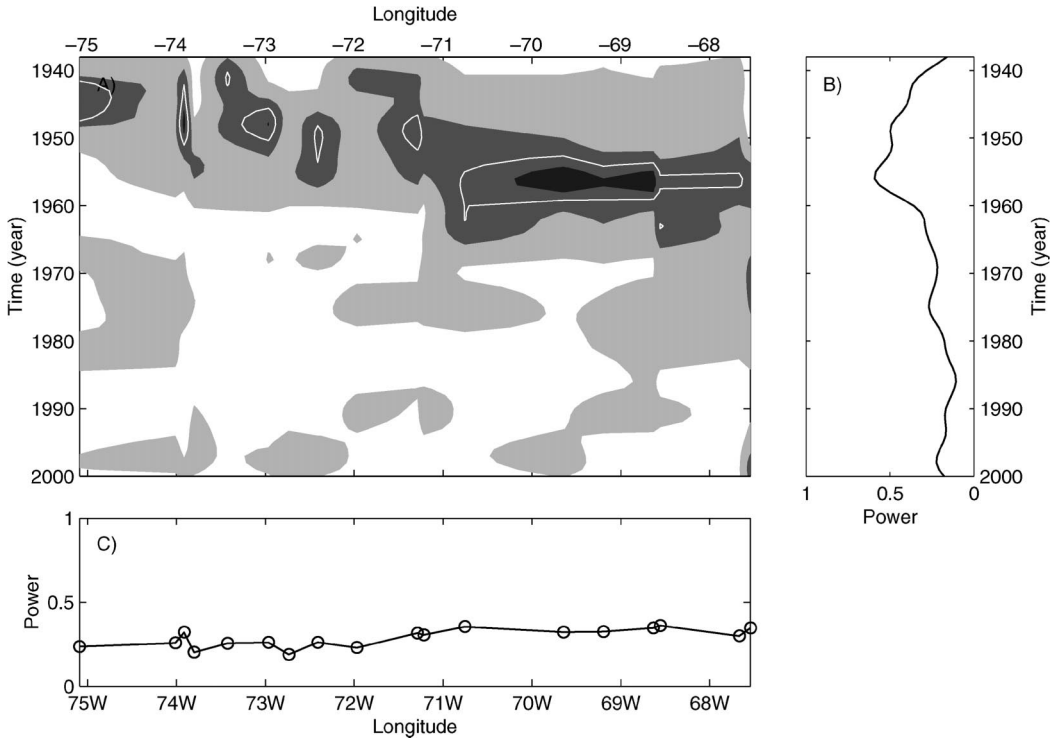

FIG. 5. Time–longitude diagrams of the streamflow observations in the 3–6-yr band. Features same as in Fig. 4.

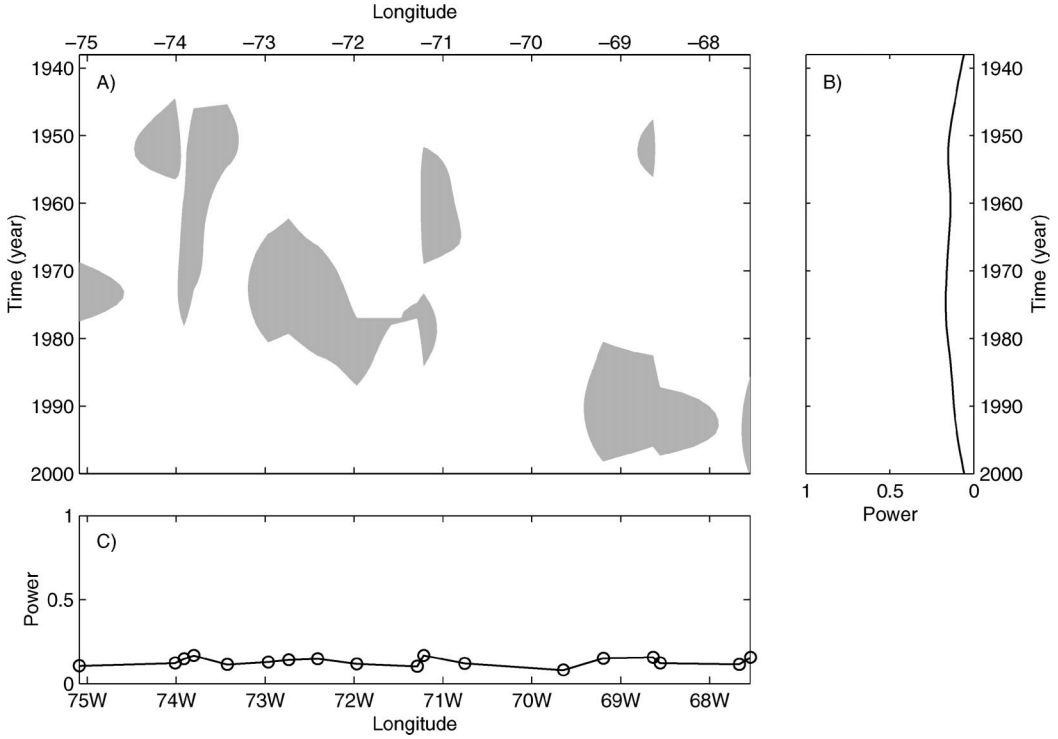

FIG. 6. Time–longitude diagrams of the streamflow observations in the 6–12-yr band. Features same as in Fig. 4.

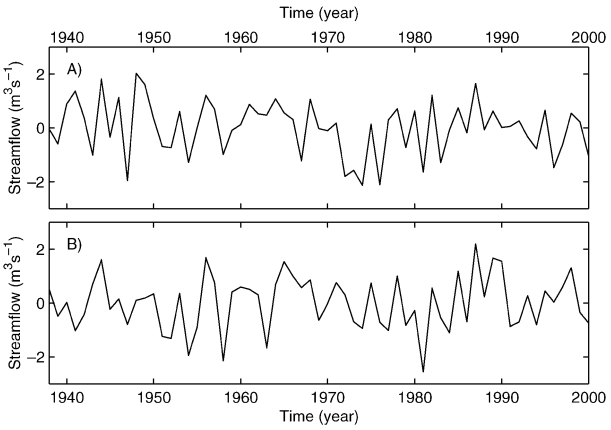

FIG. 7. Time series of streamflow leading principal component: (a) west, (b) east.

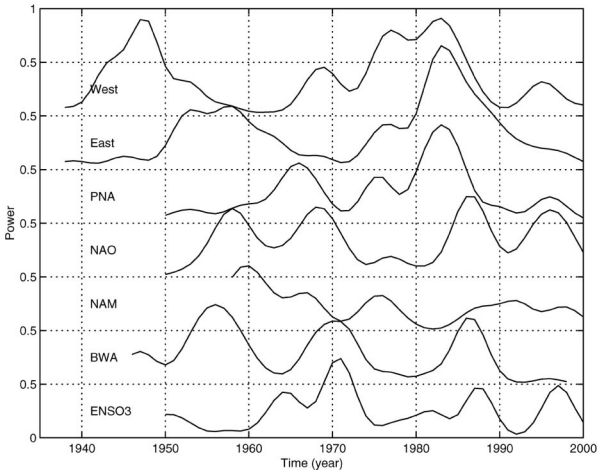

FIG. 8. Time series of the scale-averaged wavelet power for the 2–3-yr band: west, east, PNA, NAO, NAM, BWA, and ENSO3.

power spectra for PC streamflow and teleconnection series considered in this study: west, east, PNA, NAO, NAM, BWA, and ENSO3. The most striking difference between west and east powers are during the 1940s and 1950s, where they present opposite behavior in activity level. However, interannual streamflow activity in the 1940s cannot be investigated in regard to teleconnections since most of them are not available for that period. Figure 8 reveals a positive correlation between PNA activity and both streamflow activity, especially since about 1970. Correlation values are presented in Table 2, for all available data, for data prior to 1970, and for data since 1970. Considering the complete dataset, east and west are positively correlated to the PNA (0.70 and 0.69, respectively) and west is negatively correlated with the NAM (−0.57). However, if 1970 is assumed as a change point year, the picture becomes more complex. West is negatively correlated with NAM prior to 1970 (−0.70), and positively correlated with PNA afterward (0.85). East is correlated to NAM (0.85) and ENSO3 (−0.82) and less correlated to the PNA (−0.69) prior to 1970, and positively correlated to the PNA afterward (0.96). The NAO is not correlated to both streamflow power, and the BWA only shows some positive correlation prior to 1970 with east (0.45). West and east activity level in the 2–3-yr band are thus depicted by the PNA and the NAM, especially well if 1970 is assumed as a change point year. Note that the NAM series only starts in 1958, while most others start in 1950.

A similar analysis has been performed for the 3–6-yr band (Fig. 9 and Table 2). Here again, most of the activity occurs in the 1940s and 1950s, when teleconnection series are partly incomplete. Note also the increasing level of activity of the NAO and of the ENSO3 during the 1950–2000 period. Correlation based on all the available data is moderate at most: west is mainly correlated to the PNA (−0.52), but also the NAM (−0.43), and the ENSO3 (−0.42); east is mainly correlated with ENSO3 (−0.61) and PNA (−0.56). Stronger correlation are obtained when again 1970 is assumed a change point year. Then, west activity is correlated to the NAM (0.50), the BWA (0.49), and the NAO (0.46) prior to 1970, and strongly correlated only to PNA

TABLE 2. Correlation analysis results.

Teleconnection patterns	West			East		
	All	≤1970	≥1970	All	≤1970	≥1970
			2–3 yr band			
PNA	0.70	−0.10	0.85	0.69	−0.69	0.96
NAO	−0.30	−0.17	−0.36	−0.14	−0.27	−0.11
NAM	−0.57	−0.70	−0.42	−0.32	0.85	−0.49
BWA	−0.16	−0.12	−0.03	0.10	0.45	0.11
ENSO3	−0.05	0.34	−0.25	−0.32	−0.82	−0.27
			3–6 yr band			
PNA	−0.52	0.31	−0.81	−0.56	−0.25	−0.25
NAO	−0.15	0.46	0.00	−0.42	0.52	−0.77
NAM	−0.43	−0.50	−0.57	−0.29	−0.89	−0.34
BWA	0.15	0.49	−0.31	−0.06	0.23	−0.48
ENSO3	−0.42	0.02	−0.23	−0.61	0.01	−0.68

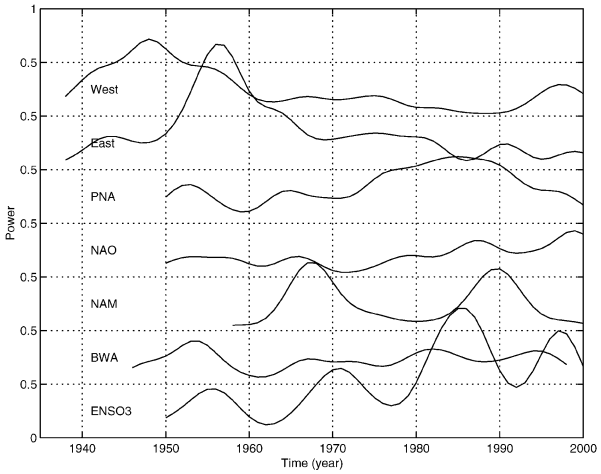

FIG. 9. Time series of the scale-averaged wavelet power for the 3–6-yr band: west, east, PNA, NAO, NAM, BWA, and ENSO3.

(−0.81) afterward. East activity is strongly correlated to the NAM (−0.89) prior to 1970, but to the NAO (−0.77) and to the ENSO3 (−0.68) afterward. A striking element in those results is the diversity of response, all teleconnection patterns being involved at some point as the main explanation of the 3–6-yr band streamflow activity, giving a complex picture of mixed teleconnections.

It is noteworthy, from Figs. 8 and 9, that the scale-averaged power of the NAO and the NAM differ considerably, even if according to Wallace (2000) they are two representation of the same phenomenon. Correlation between both indices is 0.22 for the 2–3-yr band, and −0.05 for the 3–6-yr band. This apparent discrepancy may be due to the fact that we are using mean annual indexes and not winter (December–February) indexes as in Wallace (2000).

The presence of a change point in northern midlatitude time series have been reported by other investigators. For instance, Kiely (1999) examined 5 decades of hourly precipitation (eight sites) and daily streamflow (four sites) in Ireland using the nonparametric Mann–Whitney–Pettitt test. He found a significant increase in precipitation and streamflow after 1975. This behavior was associated with the NAO, which also exhibits a similar change point. Chen and Rao (2002) tested the stationarity of midwestern U.S. hydrologic time series through a segmentation analysis, and identified change points between 1960 and 1970. Perreault et al. (2000) used a Bayesian methodology to identify a change point in the annual series of reservoir energy inflows for the Outaouais basin located immediately northwest of the present study area. They reported a change point around 1979 with approximately 12 yr of standard deviation. Finally, Shabbar et al. (1997b) identified a detectable cooling in winter surface temperature data from 12 stations on coastal eastern Canada and western Greenland since 1970 that was linked to an enhancement of the negative phase of the NAO mode and of the positive phase of the PNA. The change point around 1970, suggested by the present results, opens a slightly different perspective. Change points may not only reflect sudden changes in the intensity of climatic patterns, as depicted by teleconnection indices, they may also be attributed to modifications in the dominating climatic pattern that affects a specific region. Of course, this needs further investigation to be substantiated, but it is clear in the present analysis that the west and east 2–3-yr bands are positively correlated to PNA since 1970, which was not the case prior to that change point. The proposed simple regional east–west divide is particularly evident prior to 1970, with a negative NAM correlation for the west and a positive NAM (and negative ENSO3) for the east. The picture for the less energetic 3–6-yr band is mixed, with alternating dominancy of teleconnection patterns, but the 1970 change point holds.

5. Conclusions

Wavelet spectrum, from continuous wavelet transform, was used to describe the interannual variability in 18 contiguous southern Québec annual streamflow time series. Observed interannual activity (variance) was organized in preferential bands of wavelet periods (here, equivalent to Fourier periods), namely 2–3, 3–6, 6–16, and beyond 16 yr. However, the span of available observations, 1938–2000, has prevented looking much further than periods of about 12 yr, thus only three bands of wavelet periods were examined in greater details: 2–3, 3–6, and 6–12. This was achieved mainly by scale-averaged wavelet power spectra at multiple locations, simultaneously assessing the spatial and temporal variability of the streamflow data. The 2–3-yr band showed the highest level of activity, accounting for about 40% of the variance at each site, with peaks between 1945 and 1950 and again between 1975 and 1985. The 3–6-yr band had an activity level reaching about 25%–30% of the variance at each site. It was characterized by a peak of activity ranging from 1940 to 1960 and no organized activity for the last 40 yr. Finally, the 6–12-yr band activity essentially consisted of white noise, accounting for only about 10% of the variance at each site, and for those reasons was not be considered further in this study. However, the most striking feature in all those spectra was a net distinction between the timing of the interannual variability in local western and eastern streamflows. This opened up the opportunity to construct two regional time series, from principal component (PC) analysis, that were used to identify links with probable teleconnection pattern time series.

In general, correlation between regional streamflows and climatic indices was improved when a change point year, roughly estimated at 1970, is taken into account. For the 2–3-yr band, west was negatively correlated to the NAM prior to 1970, and positively to the PNA afterward. East was positively correlated to the NAM and

negatively correlated to the ENSO3 and the PNA prior to 1970, and positively correlated to the PNA afterward. The two predominant patterns for displaying low-frequency variability in the Northern Hemisphere, the PNA, and the NAM (or the NAO), were thus seen to alternate dominance over southern Québec, as long as the concept of change point year is validated. For the 3–6-yr band, much stronger correlations were obtained when the 1970 change point was assumed, than for the time series as a whole. West activity was moderately positively correlated to the BWA and the NAO prior to 1970, and strongly negatively correlated to PNA afterward. East activity was strongly negatively correlated to the NAM prior to 1970, and less strongly negatively correlated to the NAO and to the ENSO3 afterward. A striking element in those results was the alternate influence of the different climatic patterns. However, it is noteworthy that many climatic indices are relatively interlinked over some time period. Therefore, some suitable combination of climatic indices could have been considered. Also, the large temporal difference in variability in west and east streamflows, especially prior to 1970, was an outstanding example of the variability of (regional) streamflow response to broad climatic pattern fluctuations.

Acknowledgments. This work was made possible through a grant from the Natural Sciences and Engineering Research Council of Canada to the first author. The authors gratefully acknowledge the student contribution of Alexandrine Vallot, and Dr. Van Diem Hoang for providing the most recent streamflow observations. Main wavelet analysis routines were provided by C. Torrence and G. P. Compo, and are available at URL: http://paos.colorado.edu/research/wavelets/. The NAO, PNA, and ENSO3 indices are available through NOAA's Climate Prediction Center at URL: http://www.cpc.ncep.noaa.gov/. The AO index values are available through D. W. J. Thompson's Annular Modes Web site at URL: http://www.atmos.colostate.edu/ao/. A. Shabbar kindly provided the BWA index values. Laurence Smith and an anonymous reviewer provided many valuable comments to the manuscript.

REFERENCES

Amarasekera, K. N., R. F. Lee, E. R. Williams, and E. A. B. Eltahir, 1997: ENSO and the natural variability in the flow of tropical rivers. *J. Hydrol.,* **200,** 24–39.

Barnston, A. G., and R. E. Livezey, 1987: Classification, seasonality and persistence of low-frequency atmospheric circulation patterns. *Mon. Wea. Rev.,* **115,** 1083–1126.

Brown, R. D., 1995: Spatial and temporal variability of North American snow cover, 1971–1992. *Proc. 52nd Eastern Snow Conf.,* Toronto, Canada, 69–78.

——, and B. E. Goodison, 1996: Interannual variability in reconstructed Canadian snow cover, 1915–1992. *J. Climate,* **9,** 1299–1318.

Cayan, D. R., 1992: Latent and sensible heat flux anomalies over the Northern Oceans: The connection to monthly atmospheric circulation. *J. Climate,* **5,** 354–369.

Chen, H. L., and A. R. Rao, 2002: Testing hydrologic time series for stationarity. *J. Hydrol. Eng.,* **7,** 129–136.

Cook, E. R., R. D. D'Arrigo, and K. F. Briffa, 1998: A reconstruction of the North Atlantic Oscillation using tree-ring chronologies from North America and Europe. *Holocene,* **8,** 1–9.

Coulibaly, P., F. Anctil, P. Ramussen, and B. Bobée, 2000: A recurrent neural networks approach using indices of low-frequency climatic variability to forecast regional annual runoff. *Hydrol. Processes,* **14,** 2755–2777.

Diaz, H. F., M. P. Hoerling, and J. K. Eischeid, 2001: ENSO variability, teleconnections and climate change. *Int. J. Climatol.,* **21,** 1845–1862.

Dracup, J. A., and E. Kahya, 1994: The relationships between U.S. streamflow and La Niña events. *Water Resour. Res.,* **30,** 2133–2141.

Eltahir, E. A. B., 1996: El Niño and the natural variability in the flow of the Nile River. *Water Resour. Res.,* **32,** 131–137.

Gutiérez, F., and J. A. Dracup, 2001: An analysis of the feasibility of long-range streamflow forecasting for Columbia using El Niño–Southern Oscillation indicators. *J. Hydrol.,* **246,** 181–196.

Higuchi, K., J. Huang, and A. Shabbar, 1999: A wavelet characterization of the North Atlantic Oscillation variation and its relationship to the North Atlantic sea surface temperature. *Int. J. Climatol.,* **19,** 1119–1129.

Hu, Q., C. M. Woodruff, and S. E. Mudrick, 1998: Interdecadal variations of annual precipitation in the central United States. *Bull. Amer. Meteor. Soc.,* **79,** 221–229.

Huang, J., K. Higushi, and A. Shabbar, 1998: The relationship between the North Atlantic Oscillation and the El Niño–Southern Oscillation. *Geophys. Res. Lett.,* **25,** 665–668.

Hurrell, J. W., 1995: Decadal trends in the North Atlantic Oscillation: Regional temperature and precipitation. *Science,* **269,** 676–679.

Kahya, E., and J. A. Dracup, 1993: U.S. streamflow patterns in relation to the El Niño/Southern Oscillation. *Water Resour. Res.,* **29,** 2491–2503.

Kiely, G., 1999: Climate change in Ireland from precipitation and streamflow observations. *Adv. Water Resour.,* **23,** 141–151.

Kiem, A. S., and S. W. Franks, 2001: On the identification of ENSO-induced rainfall and runoff variability: A comparison of methods and indices. *Hydrol. Sci. J.,* **46,** 715–727.

Labat, D., R. Ababou, and A. Mangin, 2000, Rainfall-runoff relations for karstic springs. Part II: Continuous wavelet and discrete orthogonal multiresolution analyses. *J. Hydrol.,* **238,** 149–178.

Lamb, P. J., and R. A. Peppler, 1987: North Atlantic Oscillation: Concept and application. *Bull. Amer. Meteor. Soc.,* **68,** 1218–1225.

Lucero, O. A., and N. C. Rodriguez, 1999: Relationship between interdecadal fluctuations in annual rainfall amount and annual rainfall trend in a southern mid-latitudes region of Argentina. *Atmos. Res.,* **52,** 177–193.

McKerchar, A. I., C. P. Pearson, and M. E. Moss, 1996: Prediction of summer inflows to lakes in the Southern Alps, New Zealand, using the spring Southern Oscillation index. *J. Hydrol.,* **184,** 175–187.

Moss, M. E., C. P. Pearson, and A. I. McKerchar, 1994: The Southern Oscillation index as a predictor of the probability of low streamflows in New Zealand. *Water Resour. Res.,* **30,** 2717–2713.

National Research Council, 1998: *Decade-to-Century-Scale Climate Variability and Change: A Science Strategy.* National Academy Press, 142 pp.

Perreault, L., J. Bernier, B. Bobée, and E. Parent, 2000: Bayesian change-point analysis in hydrometeorological time series. Part 1. The normal model revised. *J. Hydrol.,* **235,** 221–241.

Piechota, T. C., and J. A. Dracup, 1999: Long-range streamflow forecasting using El Niño–Southern Oscillation indicators. *J. Hydrol. Eng.,* **4,** 144–151.

——, ——, and R. G. Fowell, 1997: Western U.S. streamflow and atmospheric circulation patterns during El Niño–Southern Oscillation (ENSO). *J. Hydrol.,* **201,** 249–271.

——, F. H. S. Chiew, and J. A. Dracup, 1998: Seasonal streamflow

forecasting in eastern Australia and the El Niño–Southern Oscillation. *Water Resour. Res.*, **34,** 3035–3044.
Rajagopalan, B., and U. Lall, 1998: Interannual variability in western U.S. precipitation. *J. Hydrol.*, **210,** 51–67.
Rasmusson, E. M., and T. H. Carpenter, 1982: Variations in tropical sea surface temperature and surface wind fields associated with the Southern Oscillation/El Niño. *Mon. Wea. Rev.*, **110,** 354–384.
Redmond, K. T., and R. W. Koch, 1991: Surface climate and streamflow variability in the western United States and their relationships to large-scale circulation indices. *Water Resour. Res.*, **27,** 2381–2399.
Serreze, M. C., and Coauthors, 2000: Observational evidence of recent change in the northern high-latitude environment. *Climate Change*, **46,** 159–207.
Shabbar, A., B. Bonsal, and M. Khandekar, 1997a: Canadian precipitation patterns associated with the Southern Oscillation. *J. Climate*, **10,** 3016–3027.
——, K. Higuchi, W. Skinner, and J. L. Knox, 1997b: The association between the BWA index and winter surface temperature variability over eastern Canada and west Greenland. *Int. J. Climatol.*, **17,** 1195–1210.
Smith, J. A., 1992: Representation of basin scale in flood peak distribution. *Water Resour. Res.*, **28,** 2993–2999.
Smith, L. C., D. Turcotte, and B. L. Isacks, 1998: Stream flow characterization and feature detection using a discrete wavelet transform. *Hydrol. Processes*, **12,** 233–249.
Thompson, D. W. J., and J. M. Wallace, 1998: The Arctic Oscillation signature in the wintertime geopotential height and temperature fields. *Geophys. Res. Lett.*, **25,** 1297–1300.
——, and ——, 2000: Annular modes in the extratropical circulation. Part I: Month-to-month variability. *J. Climate*, **13,** 1000–1016.
——, and ——, 2001: Regional climate impacts of the Northern Hemisphere annular mode and associated climate trends. *Science*, **293,** 85–89.
Torrence, C., and G. P. Compo, 1998: A practical guide to wavelet analysis. *Bull. Amer. Meteor. Soc.*, **79,** 61–78.
——, and P. J. Webster, 1999: Interdecadal changes in the ENSO–Monsoon system. *J. Climate*, **12,** 2679–2690.
Wallace, J. M., 2000: North Atlantic Oscillation/annular mode: Two paradigms—One phenomenon. *Quart. J. Roy. Meteor. Soc.*, **126,** 791–805.
——, and D. S. Gutzler, 1981: Teleconnections in the geopotential height field during the Northern Hemisphere winter. *Mon. Wea. Rev.*, **109,** 784–812.
Waylen, P., and C. Caviedes, 1990: Annual and seasonal fluctuations of precipitation and streamflow in the Aconcagua River basin, Chile. *J. Hydrol.*, **120,** 79–102.
Woo, M., R. Heron, P. Marsh, and P. Steer, 1983: Comparison of weather station snowfall with winter snow accumulation in high Arctic basins. *Atmos.–Ocean*, **21,** 312–325.
Yarnal, B., and H. F. Diaz, 1986: Relationships between the extremes of the Southern Oscillations and the winter climate of the Anglo-American Pacific coast. *Int. J. Climatol.*, **6,** 197–219.